Landscape Ecol
DOI 10.1007/s10980-010-9450-9

RESEARCH ARTICLE

Landscape patterns in boundary intensity: a case study of mussel beds

Carlos D. Robles · Corey Garza · Robert A. Desharnais · Megan J. Donahue

Received: 2 May 2009 / Accepted: 2 January 2010

Abstract This work examines the proposition that positive interactions among neighboring individuals within a population may produce landscape patterns in boundary intensity. The large scale patterns emerge because the interactions favor an aggregated distribution in the face of a potential limiting factor, and the strength of that factor varies over the landscape. The consequences of spatially varying neighborhood processes were explored using cellular automata simulating the structure of mussel beds in 2-dimensional intertidal landscapes, each characterized by a vertical gradient of tidal immersion and a horizontal gradient of wave energy. Running the model with and without the neighborhood processes demonstrated that the facilitating neighborhood processes elevate intensity above that caused by the gradients, and consequently abrupt (high intensity) boundaries emerged in the midst of gradual environmental variation. Trends generated on the 2-D landscape by the model were compared with those in photo-mosaics of intertidal mussel beds, *Mytilus californianus* on rocky shores of the British Columbia. The analysis involved interpolation of boundary locations using a spatially-constrained cluster algorithm, and then estimation of the corresponding boundary intensities using a landscape index aggregation (CLUMPY). The general similarity between predicted and real trends in intensity over the wave energy gradients suggests that spatially varying neighborhood processes determine much of the landscape scale variation in boundary intensity, while certain discrepancies (e.g. a more rapid rise of observed intensities with increasing wave exposure) suggest modifications of the theory and new empirical work.

Keywords Boundary intensity · Cellular automata · CLUMPY · Facilitation · *Mytilus* sp. · Neighborhood effect · Photo-mosaic · Scale · Spatially-constrained cluster algorithm

Electronic supplementary material The online version of this article (doi:10.1007/s10980-010-9450-9) contains supplementary material, which is available to authorized users.

C. D. Robles (✉) · C. Garza · R. A. Desharnais · M. J. Donahue
Department of Biological Sciences, California State University at Los Angeles, Los Angeles, CA 90032, USA
e-mail: crobles@calstatela.edu

Present Address:
C. Garza
Division of Science and Environmental Policy, California State University Monterey Bay, Seaside, CA 93955, USA

Present Address:
M. J. Donahue
Hawaii Institute of Marine Biology, University of Hawaii, PO Box 1346, Kaneohe, HI 96744, USA

Introduction

Quantitative theory (e.g. Wilson et al. 1996; Wilson and Nisbet 1997; Vandermeer and Yodis 1999; Robles and Desharnais 2002; van de Koppel et al.

Published online: 23 January 2010

2005) proposes dynamics that generate landscape patterns of boundary intensity (sharpness and contrast; *sensu* Strayer et al. 2003). The boundaries of a population fall along lines in the landscape where spatial gradients in rates of loss (predation, competition, or other risks) exceed the corresponding gain (recruitment and growth). A stable boundary marks a phase shift in an equilibrium between gain and loss, from one outside the boundary yielding low densities of newly recruited juveniles, to one inside the boundary yielding high densities of mixed age classes. In the simplest dynamics, sharp (high intensity) boundaries form where environmental discontinuities cause an abrupt spatial shift in the components of the equilibrium. Diffuse (low intensity) boundaries form within slowly changing environmental gradients (Turner 1989).

The formative dynamics of intensity become more complex when, in addition to the large-scale environmental gradients, small-scale interactions among neighboring individuals modify components of the equilibrium. For example, positive neighborhood effects may allow aggregations to survive risks intolerable to solitary individuals. A population initially seeded in relatively favorable environmental conditions may thus expand into a gradient of increasing risk (physical stress, predation, or other mortality factors), the advancing boundary intensifying as the survival of solitary individuals diminishes and individuals in the aggregation continue to flourish and reproduce. The boundary advances until it reaches a point at which further increases in risk cannot be accommodated by the facilitating neighborhood process, forming a sharp stationary boundary. Thus, remarkably, such neighborhood processes produce sharp boundaries within slowly changing environmental gradients (O'Neill et al. 1989; Gosz 1993; Risser 1995; Wilson et al. 1996; Wilson and Nisbet 1997; Vandermeer and Yodis 1999).

Recent field studies describe many possible examples of the facilitating neighborhood processes in terrestrial and marine landscapes (reviews in Wilson and Agnew 1992; Bruno et al. 2003; Harley 2007). Among them, mussel beds on sea shores stand out as an especially apt system for study, because the factors setting their upper and lower vertical boundaries have been repeatedly investigated with controlled experiments, and much is known about mussel ecology.

Field experiments have demonstrated facilitating interactions among neighboring mussels. While juvenile mussels may settle out from the water column onto any rough surface, rates of juvenile recruitment are often greater under and around larger mussels, and the number of recruits under an established mussel is positively correlated with its size (e.g. *Geukensia demissa*, Bertness and Grosholtz 1985; Nielson and Franz 1995; *Mytilus californianus*, Robles unpublished data). In areas where predators are active, large, predator-resistant mussels shield otherwise vulnerable juveniles and small adults within the aggregations (e.g. *Geukensia demissa*, Bertness and Grosholtz 1985; *Mytilus californianus*; Fong and Robles, unpublished data). Thus, facilitating neighborhood processes are implicated in the establishment and survival of small mussels.

In the case of the sea mussel *Mytilus californianus*, experimental manipulations of the densities of predatory sea stars (*Pisaster ochraceus*; Paine 1974; Robles et al. 2009) revealed the operation of intense size-dependent predation in the equilibria maintaining lower boundaries. Under natural conditions, the lower boundaries are usually comprised of a matrix of large predator-resistant mussels with smaller, younger mussels underneath. When sea stars were held to abnormally low densities by experimental reductions, mussel recruits accumulated on top of the lower boundary mussels and at shore levels below. The few remaining sea stars consumed small mussels to the exclusion of large (Robles et al. 2009). However, when sea star densities were experimentally boosted far above natural levels, all small prey species at lower shore levels were depleted, and the proportion of large mussels in sea star diets increased. Very large mussels comprising the matrix of the lower boundary were consumed along with the smaller mussels underneath them, and the lower boundary receded upwards. The boundaries on control sites remained unchanged for a period of years (Robles et al. 2009). Thus, facilitating neighborhood processes appear to be an integral part of the equilibria maintaining lower boundaries.

Different processes occur at the upper boundaries. The prolonged periods of emergence at high shore levels limits mussel growth, and the maximum sizes of mussels are a fraction of those at lower levels (Dehnel 1956; Kopp 1979; this study). Prolonged

emergence also severely restricts sea star foraging. Rather than size-dependent predation, mortality from physical stress (elevated temperature and desiccation; Paine 1974; Harley 2007) apparently sets the upper boundary. Here again facilitating neighborhood processes may play a role, if settlement and initial survival is enhanced in the moist "footprint" of established mussels (discussion in Bertness and Leonard 1997; Harley 2007).

Assuming for the moment that facilitating neighborhood processes do affect the boundaries of sea mussel beds, then one would expect boundary intensities to be greater than that determined by the environmental gradients alone. One might also expect lower boundaries to be relatively more intense than upper boundaries, because on the low shore severe size-limited predation is met with high mussel recruitment and rapid growth to large resistant sizes, accentuating neighborhood effects. On the upper shore, predation is negligible, while mussel settlement, growth rates, and final sizes are greatly curtailed by prolonged tidal emergence, constraining the neighborhood effect on recruitment. Thus, as mussel productivity declines toward progressively higher shore levels gaps among the aggregations proliferate.

Although theory predicts such variation, no prior empirical studies have quantified landscape patterns of intensity, much less tied them to specific environmental factors modulating the strength of the neighborhood effects. Recent advances in spatially explicit modeling and the statistical characterization of boundaries present an opportunity to advance our understanding of this aspect of landscape dynamics (Fagan et al. 2003).

We use cellular automata (CA model; Robles and Desharnais 2002; Donalson et al. 2004) to explore relationships between neighborhood processes and landscape-scale trends in boundary intensity. The model is run without and with facilitating neighborhood processes. Comparisons among the different runs of the model illustrate how these process may generate spatial tends in boundary intensity. Then, a comparison of simulated and real trends is made by applying the same spatial analysis to the two-dimensional landscapes output by the CA model and to photo-mosaic images of mussel beds. Specific correspondences between simulated and real trends suggest that boundary intensities do vary with the neighborhood processes, while certain discrepancies suggest modifications of theory and further empirical work.

Methods

The CA model

Here we provide a brief general description of the model. Model expressions and the empirical evidence for them appear in Appendix I, Supplemental Materials (see also Robles and Desharnais 2002; Donalson et al. 2004).

The CA Model depicts the intertidal landscape as a rectangular grid of cells with each cell representing a position potentially occupied by a mussel. A state matrix of numbers (0 = absent; 1 = recruits 1 mm long; 2 = 2 mm long, etc.) keeps track of the size structure of the bed at any instant (time step). A time step advances by multiplying the state matrix times a transition probability matrix expressing the likelihood of the biological events occurring in each cell (i.e. position-specific recruitment, growth to a larger size, predation, and other mortality).

The transition probabilities vary along the vertical and horizontal dimensions, representing spatial variation in vital rates over gradients of tidal immersion and wave energy (flow speed). These two aspects of intertidal water motion influence the productivity of mussels by determining the duration and rate of impingement of larvae and food particles on the rock surface. Larvae competent to settle are concentrated near the surface, so that settlement rates along the vertical gradient of immersion follow a unimodal curve with the peak at mid shore levels. The height of the peak (maximum settlement) depends on wave energy, which may vary in the horizontal dimension. Mussel growth increases towards lower shore levels (i.e. greater immersion) and higher wave energy (i.e. greater nutrient exchange). Immersion time and flow speed also affect the intensity of predation because sea stars are intolerant of low tide exposures, and their foraging during high tide is hindered in high wave energies by hydrodynamic stresses.

The neighborhood effect is imposed by weighting the transition probabilities of a given cell by the occupancy of the neighboring cells, such that, for example, a small mussel surrounded by larger

mussels has a lower probability of predation than a small solitary mussel. Similarly, an empty cell adjacent to cells occupied by large mussels has a higher probability of recruitment.

Predation dynamics are modeled as a stochastic immigration-emigration process. A single global variable describes predator density (although predator attack rates vary in space as described above). Predators enter the CA at a constant rate, but emigration probabilities are inversely proportional to the per capita consumption rate of prey.

Over successive time steps, effects of the gradients interact with effects of the neighborhood process until a steady state is reached, in which the overall spatial pattern of sizes (trends within the state matrix) remains constant while the occupancy of individual cells turns over. See Appendix I for further explanation of the model parameterization.

It should be noted that storm waves rip gaps in mussel beds. The propagation of such mechanical disturbance through mussel beds can be analyzed as another neighborhood process (Guichard et al. 2003). However, our purpose was to examine intact boundaries. The model therefore omits effects of mechanical disturbance, and the field sampling focused on undisturbed boundaries, which constituted >90% of the total boundary lengths. Gaps could be distinguished from predatory losses because they formed abruptly in the stormy winter through early spring period, when the sea stars were inactive.

Model scaling: within-site and among-sites versions of the model

Wave energies show substantial variation along the shoreline. We used the beds themselves to define two relevant sampling scales: within-site (1–10 m) and among-sites (10–100 s of meters). For the within-site scale, advancing wave fronts approach the rock face at an oblique angle, forming a steep gradient as energy dissipates from the seaward impact surface to the landward surface. For the among-sites scale, a gradient in wave exposure occurs where separate rock benches within a region intercept different prevailing wave energies, while wave energy is comparatively uniform within a short segment of shoreline where wave fronts approach parallel to the shoreline.

We used two variations of the model to simulate within-site and among-site variation in wave energy. In the within-site version, the complete range of wave energy spanned the horizontal dimension of one grid, and this grid had a single predator population, which responded to the abundance and size-distribution of mussels within the array (site). In the among-sites version, a series of grids, one in the center of each site, was run. Each grid had a different horizontally uniform wave energy (defined by the corresponding values of the state transitions) and its own predator population.

Photo-mosaics of field populations: capturing the real patterns

Twelve mussel beds were chosen within a 10 km^2 area in Barkley Sound, British Columbia, Canada (48°53′N; 125°20′W). A photographer walked transect lines along the boundaries, taking pictures with a digital camera mounted on an armature atop a pole. The component images were later assembled into mosaics, and each mosaic was registered to its corresponding raster model of surface elevation for an individual site. For the within-site scale, a mosaic was taken of a mussel bed on a rock face receiving wave energy from an oblique angle. For the among-sites scale, 11 sites were selected, each with apparently uniform horizontal wave energy, but as a group spanning the range of apparent exposure to prevailing wave fronts. Details of the sample layouts and photo-mosaic procedures appear in Appendix II a and Blakeway et al. (2004).

Measurements of wave energy

Estimates of the wave energy were obtained with deployments of wave dynamometers (Bell and Denny 1994). These record the maximum instantaneous flow speed at the attachment spot during the period of deployment. For the within-site estimates, dynamometers were attached at 2 m intervals over the entire mosaic area. The location of each dynamometer, relative to mean lower low water (MLLW), was then measured with a Topcon Total Station surveyor (Trade mark, Topcon Corporation, Tokyo, Japan). Dynamometer readings were taken during two separate periods of three consecutive days in August. The point and flow speed data were then added into ArcMap GIS software (ESRI) and a gradient of flow speed over the area of the mosaic was interpolated as a function of horizontal distance using the raster interpolation function.

For the among-sites estimates, a pair of dynamometers was placed on each of two shore level contours, +2.1 and +3.0 m MLLW. Members of each pair straddled the vertical midline of each site and were horizontally separated by 5 m. Readings were taken on four consecutive days in August. Summer is the season of relatively low wave energies; therefore, the records underestimate the prevailing differences in flow speed among the sites. However, one would expect few errors in the relative ranking of sites, because the swells in the recording period approached the shorelines from the same direction as winter swells. The ranks of five of the sites were in perfect agreement with estimates of flow speed made by divers over longer periods on those sites as part of another study Robles et al. (1989). Therefore, we report the rank of the mean maximum flow speeds as the measure of wave energy in the analyses. Using measured flow speeds instead did not change the outcome of the statistical inferences.

Analysis of the dynamometer readings indicated that the sampling did capture the two different horizontal scales of wave energy. Flow speeds based on the interpolation ranged from 2.0 to 4.8 ms^{-1} over the horizontal span of the within-site samples. The mean flow speeds of the sites in the among-sites comparison ranged from 2.91 ± 0.27 ms^{-1} SE to $12.32.14 \pm 2.38$ ms^{-1} SE. Also in the among-sites comparison, the mean horizontal differential in flow speeds (average of the difference in speeds between left and right dynamometer positions on a site) was 1.80 ± 1.44 ms^{-1} SE. Since the horizontal span of the sample girds in the photo-mosaics was $\leq$1.5 m within the 5 m span of the drogues, it is clear that the among-sites comparison sampled a relatively small horizontal range of wave energy at each site.

One might expect that boundaries constrained by factors linked to topography would show differences boundary intensity in proportion to the slope of the surface. In the present case, steeper shores might be expected to show more intense boundaries. To control this potentially confounding effect, sites were chosen with continuous surfaces, unbroken by large crevices or tide pools, and including a similar range of slopes at the two boundary levels. As a crosscheck, clinometer readings were taken at apparent boundaries, later determined to be $<$0.5 m from the objectively delineated boundaries. The readings confirmed that slopes for lower and upper boundaries of the among-sites comparison were similar (Mean slope in degrees at lower boundary = 14.182°, SD = 5.49°; Mean slope in degrees at upper boundary = 14.273°, SD = 14.027°; $t = 0.044$, df = 20, $P = 0.965$). The same was found for the slopes in the within-site comparison (Mean lower = 13.000°, SD = 4.743°; mean upper = 12.400°, SD = 4.506°; $t = 0.205$, df = 8, $P = 0.843$.).

Measures of mussel size: mean cell states

Sample grids were superimposed on the apparent boundaries in the mosaic, and the sizes of mussels in the cells were scored. The CA model assumes a constant cell size and represents mussel sizes with integers. On the shore, however, different boundaries present mussels of different maximum size. To achieve approximately equal cell scaling across all comparisons, the cell sizes in the mosaic sample grids were scaled to mussel size. The side of a cell equaled the square root of the average of the virtual areas of the 10 largest mussels in the grid, so that most occupied cells enclosed the centroid of just one mussel. A cell's state was scored as the length (cm) of the largest mussel with its centroid in the cell. Mean states for sample grids in the mosaics and the model arrays were calculated as the average of the two rows closest to the boundary delineation.

At the upper boundaries, small *M. californianus* sometimes occurred with a superficially similar mussel *Mytilus trossulus*. A double blind test confirmed the accuracy of mussel scoring in the photo-mosaic samples (approximately 1% error; see Appendix II b for details).

Boundary location: boundary delineation and height measurements

For both the model landscapes and field mosaics, rectangular sample grids (25 rows, 15 columns) were placed straddling the apparent upper or lower boundaries. Each grid was set with the first two rows on the side closest to the midline of the mussel bed (proximal) anchored in $\geq$90% occupancy and the successive rows with lower occupancy. The two rows on the side away from the midline (distal) had $\leq$10% occupancy. Thus, the boundary fell somewhere within the grid (Fig. 1).

To objectively delineate boundaries of markedly different intensities, a conventional algorithm for spatially constrained clustering was employed (Gordon 1999; e.g. Legendre and Fortin 1989; software by Boundary Seer^{TM} TerraSeer Inc.). Successive iterations agglomerated adjacent cells of similar values until all cells were classed into one of two cluster groups, encompassing relatively high or low abundances. The cluster borders separating high and low abundance defined the mussel bed boundary (grey panels, Fig. 1). The height of a boundary for a given sample grid was estimated as the mean of 3 tidal height estimates at even intervals along the boundary delineation. For the photo-mosaics, the heights were estimated from the elevation surfaces estimated in the Arc Map raster model.

In grids with highly fragmented occupancy ("patchy" covers), it was not possible to anchor a side of the grid in ≥90% occupancy. In this case, the 25 × 15 grid was set to enclose the highest occupancy available. The outlines of the abundance clusters did not join into a continuous horizontal boundary, and therefore, the upper or lower boundary heights were estimated from the top or bottom margins of the largest high abundance clusters (mussel clumps). For grids with highly fragmented occupancy (sparse

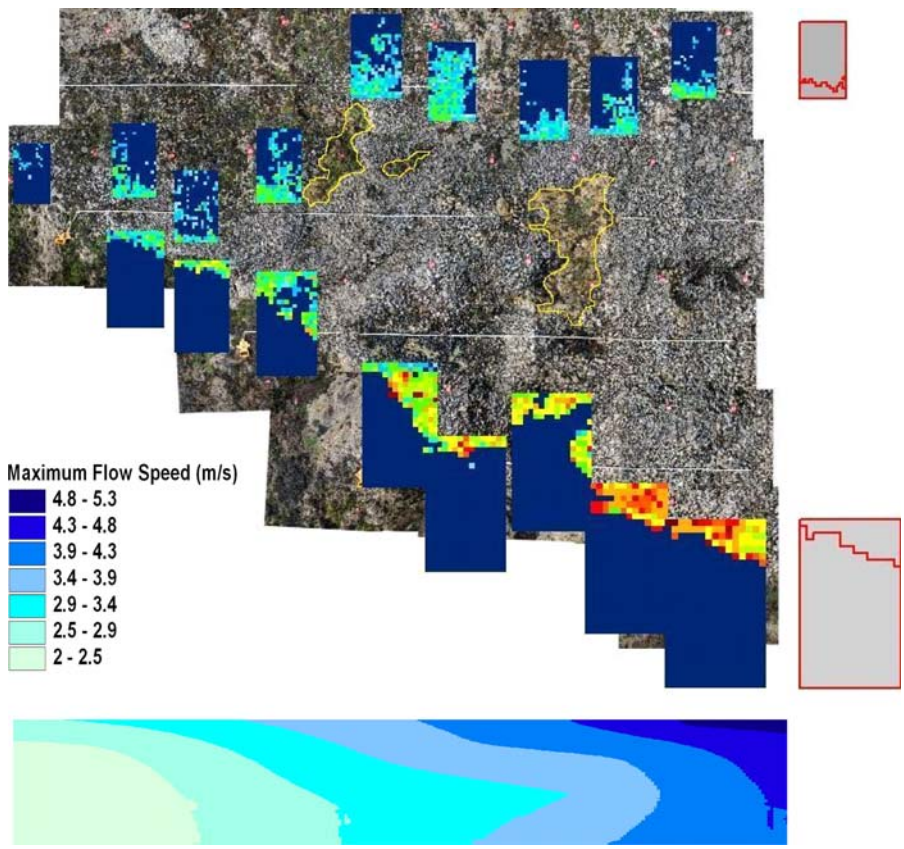

Fig. 1 Within-site photo-mosaic showing the sampling method. Sample grids are aligned along the *upper* and *lower* boundaries of the mussel bed. The maximum width of the mosaic corresponds to approximately 10 m. Cell color in the grids indicates state: *navy* = unoccupied, hues of *light blue* through *dark red* represent successively larger mussels, from 1 to 14 cm long. *Grey panels* show delineations of boundaries computed by the spatially constrained clustering algorithm for the corresponding grids to the *left*. Waves impact to the *right* of the mosaic and pass *left*. The *color bar* indicates alongshore gradient in wave energy, represented by a raster interpolation of maximum flow speeds measured by wave dynamometers. To save space in the figure, the vertical dimension of the flow speed interpolation has been compressed to 1/4th its original span. Mussel tear-outs generated earlier by winter storms are outlined in *yellow*. Elevations are difficult to perceive in the 2-D mosaic. The 5th and 6th grids from the *left* in the *upper row* fell on *lower* shore levels than the frames to their *right*, as determined by reference to a raster interpolation of elevation records

random covers), the algorithm produced numerous horizontal subdivisions without a clear dichotomy of high and low abundance. Mean state and intensity, but not boundary heights, were estimated.

Measures of boundary intensity

We employed the CLUMPY index (McGarigal et al. 2002) to measure the intensity of mussel boundaries. The CLUMPY index varies with the dispersion of a cover class in raster maps, from -1 for completely uniform dispersion, to 0 for random dispersion, to $+1$ for perfectly aggregated dispersion. CLUMPY is preferred over other commonly employed measures of fragmentation, e.g. the Aggregation Index (AI) and normalized landscape scale index (nLSI), because it shows a nearly linear (shallow hyperbolic) response to varying degrees of aggregation over a wide range of percent covers (Neel et al. 2004). For the realm of our samples (high apparent aggregation and low percent covers or low apparent aggregation and moderate per cent covers) CLUMPY should provide slightly conservative values, i.e. minimally biased against the working hypothesis. The sample grids were the same as those used in the height analysis, except that the cells were scored for presence/absence of mussels. The CLUMPY index was calculated for the presence class.

Trends in boundary measures

For both model arrays and mosaics, we examined trends in mean state, boundary height, and intensity by fitting either a linear regression model, $Y_i = b_0 + b_1 \times X_i$, or a quadratic regression model $Y_i = b_0 + b_1 \times X_i + b_2 \times X_i^2$, where Y_i is the measure, X_i is the variable representing relative wave energy, and b_0, b_1, and b_2 are the regression coefficients. A linear or quadratic least squares fit was chosen depending on which yielded the lowest P-value in an analysis of variance of a given data set.

Results

Within-site version of the model:

The state matrix approached an asymptotic distribution after a few thousand iterations. In all runs, we stopped the model after 20,000 iterations to ensure a steady-state. Spatial tends in, boundary height, mean state, and intensity were readily apparent (Fig. 2).

Boundary height estimates were not made for the lowest wave energy (WE = 0.1), because unambiguous boundaries could not be delineated using the cluster algorithm. Boundaries were well delineated for higher wave energies. Mean heights of lower and upper boundaries diverged from low to high wave energies (Fig. 3b).

Mean states (mussel lengths) at lower and upper boundaries are similarly low (2.25 cm) at the lowest wave energy, but with increasing wave energies the mean states of lower boundary grids increase more rapidly than do mean states for upper boundary grids (Fig. 3a). The range of means states is approximately 11 cm for the lower grids, but only 1.9 cm for the upper grids. The mean states are obviously related to the growth rates associated with the heights along the boundaries. We note that even though the parameterization of all transition probabilities is continuous and gradual over the gradients, the model's stochastic process yields considerable variation of points about the curves (Fig. 3a).

The apparent difference in the intensity of lower and upper boundaries (Fig. 2) was confirmed by the CLUMPY index (Fig. 3c). Lower boundaries were much more intense than upper boundaries, and with increasing wave energy CLUMPY values for the lower boundary approached the theoretical maximum for

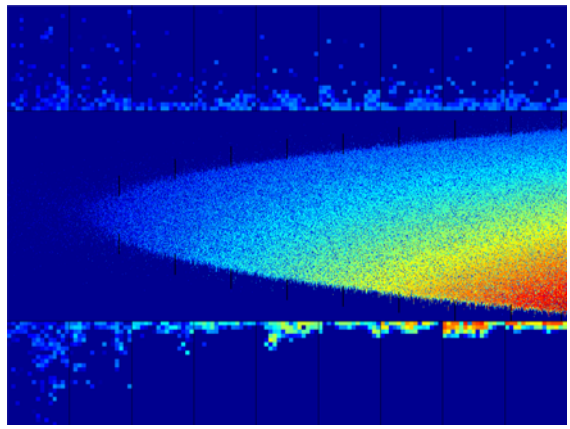

Fig. 2 Within-site version of the model, steady state array (*central panel*) with sub-sections of the boundaries magnified (*marginal panels*). *X-axis* represents the alongshore gradient in wave energy. *Y-axis* represents tidal emersion. *Pixel color* represents mussel size: *blue* through *red* for increasingly large mussels

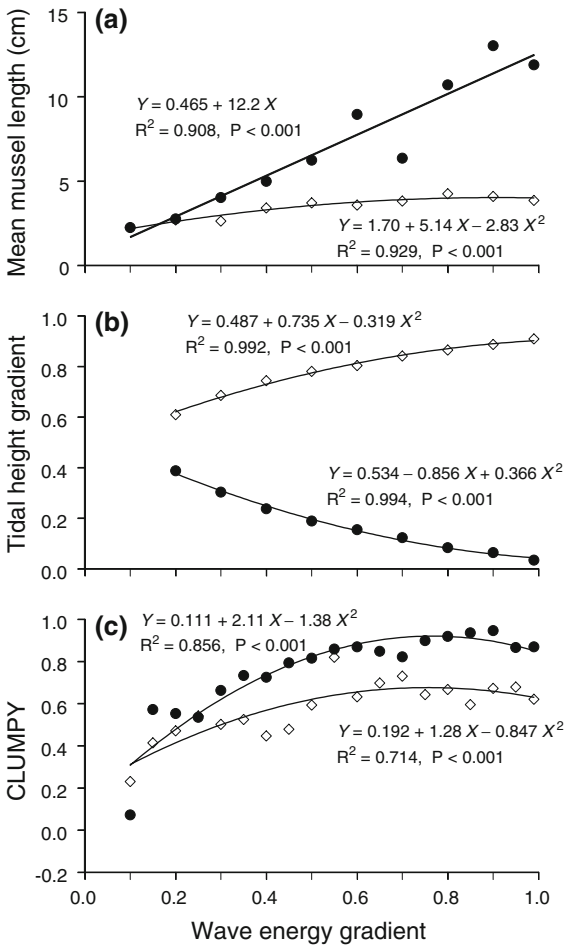

Fig. 3 **a**, **b**, **c** Regression analyses for the within-sites version of the model. Estimated equations, coefficients of determination (R^2), and levels of significance values (P) are shown for each regression of the specific measure against relative wave energy. **a** mean state; **b** boundary height (shore level); **c** CLUMPY, an index of landscape fragmentation that varies from −1 for completely uniform dispersion, to 0 for random dispersion, to +1 for perfectly aggregated dispersion. *Dots* = lower boundary estimates, *diamonds* = upper boundary estimates

aggregated cover (1.0). The intensities of the upper boundary also increased with wave energy, but to a much lesser degree (Fig. 3c). Comparison of residuals for different types of curves indicates that the increases are best described by a hyperbolic relationship.

What is the role of the neighborhood process in the model?

To assess the contribution of the neighborhood process, the within-site version was run again, but without the neighborhood weighting on recruitment and predation probabilities. Vertically diverging boundaries again appeared as the dominant feature of the steady state array (Fig. 4). Mean state (size) relationships appeared very similar to the model with neighborhood effects (Fig. 5a vs. 3a). However, unambiguous boundaries could not be delineated for grids in the lower half of the wave energy gradient (WE 0.1–0.5). Delineations of the grids at higher wave energies showed a reduced vertical range of boundaries relative to the model with the neighborhood process (Fig. 5b).

Lower and upper boundaries showed the same trend in intensity (Fig. 5c). CLUMPY values for the lowest wave energies approached the theoretical value zero for random dispersion (Fig. 5c), and CLUMPY increased slightly, but significantly with wave energy. However, values for CLUMPY without neighborhood processes were far below corresponding values with neighborhood processes operating (Fig. 5c vs. 3c). Thus, in the model the role of the neighborhood processes is to extend and intensify boundaries, but the degree to which this occurs depends on changes in the relative importance of different limiting factors and the strength of the amount of neighborhood weighing. The downward extension and intensification attributable to neighborhood effects are greatest for the lower boundary in high wave energies, where mussel are largest and

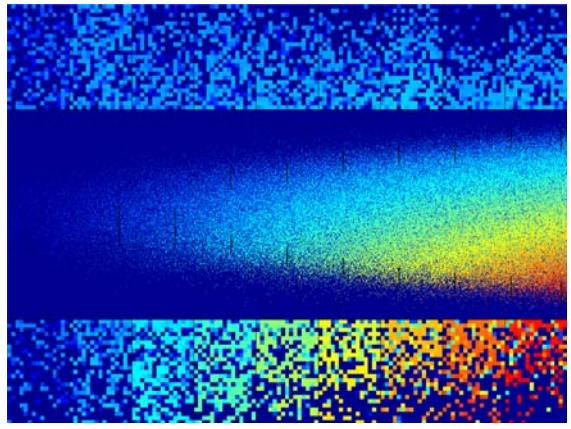

Fig. 4 Effect of removing neighborhood processes. Steady state array (*central panel*) and sub-sections of the boundaries magnified (*marginal panels*) of the within-site version of the model with the neighborhood component switched off. *Axes* as in Fig. 2

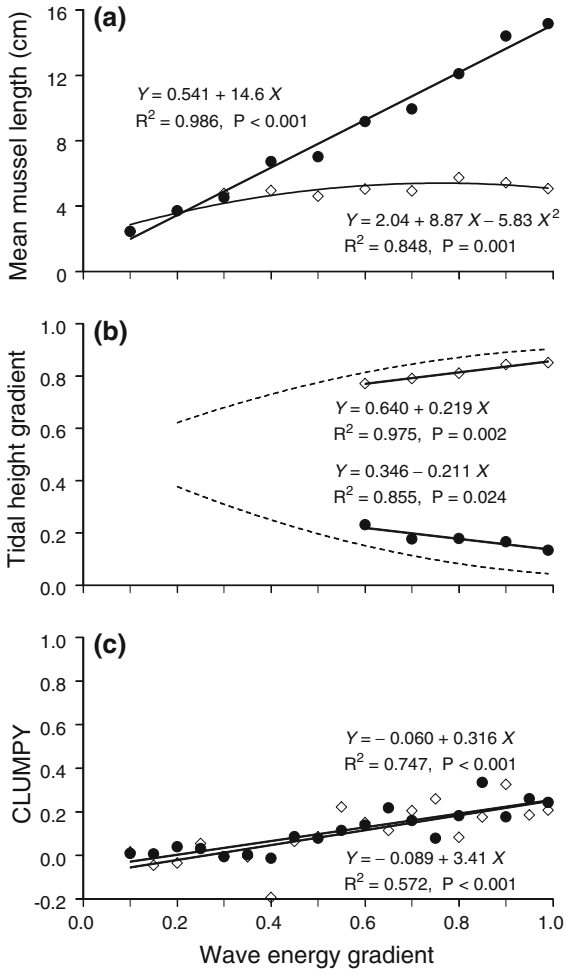

Fig. 5 **a**, **b**, **c** Analysis of model without neighborhood process. Format as in Fig. 3. **a** mean state; **b** boundary height; **c** CLUMPY. *Dots* = lower boundary estimates, *diamonds* = upper boundary estimates. For (**b**), height estimates are not available for low wave energies because unambiguous boundaries could not be delineated. *Dotted lines* show boundary height relationships for model with neighborhood effects

size-dependent predation is the primary factor setting the lower boundary.

Among-sites version of the model:

The steady state of the among-sites version of the model showed similar patterns to those of the within-site version (Fig. 6). The regressions for mean state, boundary height, or CLUMPY against wave energy were qualitatively similar to the within-site version (Fig. 7a, b, c). This not a trivial outcome; in addition

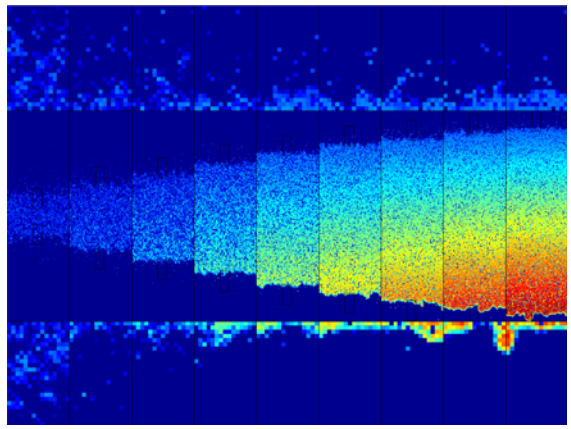

Fig. 6 Steady state array (*central panels*) with sub-regions (*squares*) magnified (*marginal panels*) of the among-sites version of the model. Panels from *left* to *right* represent runs with increasing wave energy

to the different scaling of transition probabilities along the horizontal axis, each model array in the among-site version had separate predator population dynamics. If the predator systems responded very differently to the difference in horizontal gradients, then one might not have expected the similarity in zonation patterns between the among-site and within-site versions.

Photo-mosaics of real boundaries: the within-site scale

Mean states for the lower boundary increased with wave energy, upper boundaries did not (Fig. 8a). The range of mean states for the two boundaries (lower = 5.3 cm, upper = 0.5 cm) is less than the corresponding ranges of the within-site model. The difference in the range of maximum flow speeds between this site and those used for the within-sites scale (2.8 and 9.4 ms^{-1}, respectively) indicates that the 10 m span of the mosaic sampled only a portion of the natural wave energy gradient, which might account for the smaller range of mean states.

The patchy cover of the grid at minimum wave energy (Fig. 1) did not yield continuous boundary delineation, and heights were estimated from the margins of the largest clump. Boundaries at higher wave energies were continuous, as delineated by the cluster algorithm. Mean heights of lower and upper boundaries diverged with increasing wave energy (Fig. 8b).

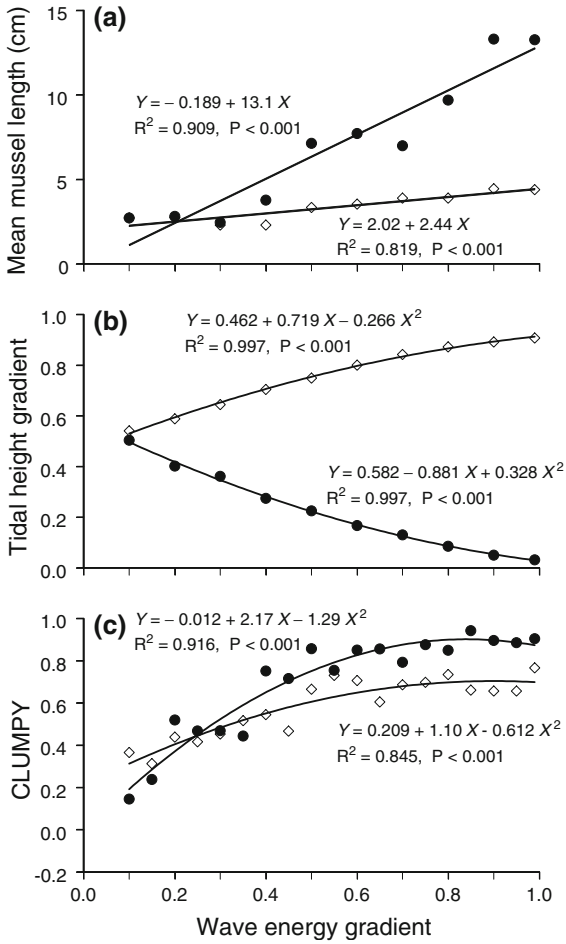

Fig. 7 **a**, **b**, **c** Regression analyses for among-sites version of the model. Format as in Fig. 3. **a** mean state; **b** boundary height; **c** CLUMPY. *Dots* = lower boundary estimates, *diamonds* = upper boundary estimates

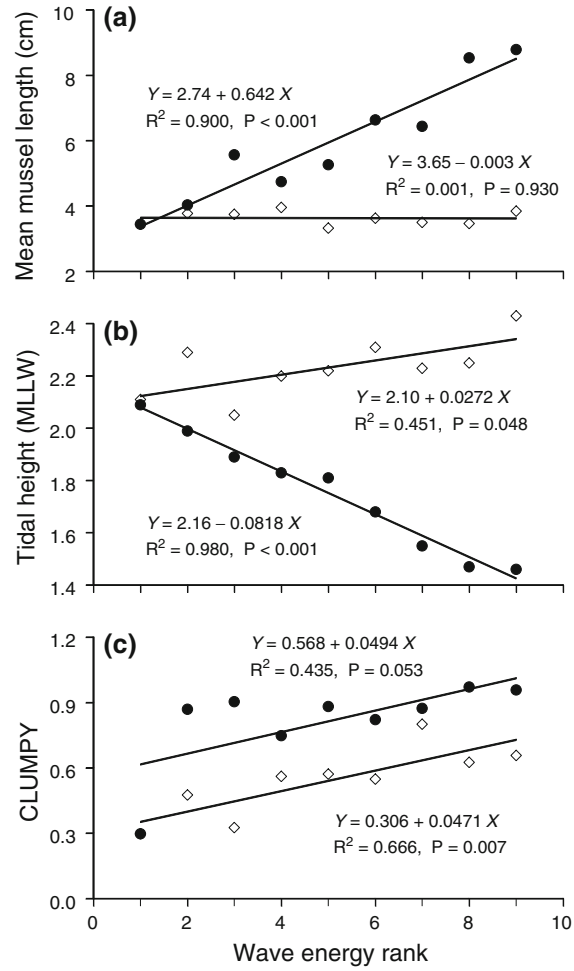

Fig. 8 **a**, **b**, **c** Regression analyses for field mosaic from the within-site sampling scale. Format is in Fig. 3. **a** mean state (cm); **b** boundary height (meters above MLLW); **c** CLUMPY. *Dots* = lower boundary estimates, *diamonds* = upper boundary estimates

Lower and upper boundaries were similarly diffuse at the lowest wave energy, but the increase in intensity with wave energy was much more rapid for the lower boundary (Fig. 8c). At highest wave energies, CLUMPY values for the lower boundary approached the theoretical maximum for aggregated distributions.

Photo-mosaics of real boundaries: the among-sites scale

Mean states for the lower boundary increased with wave energy; mean states for the upper boundary did not (Fig. 9a). The ranges of mean states for the lower and upper boundaries were 6.8 and 1.1 cm, respectively.

The patchy covers of the site with the minimum wave energy did not yield a continuous boundary, and heights were estimated for the lower and upper margins of the largest clumps. Grids on sites with higher wave energies showed continuous boundaries. As in the within-site photo-mosaic and the two complete versions of the model, the lower and upper boundaries diverged vertically towards higher wave energies (Fig. 9b).

At all but the lowest wave energy site, CLUMPY values of lower boundaries were high, and they increased significantly with increasing wave energy (Fig. 9c). CLUMPY values for the upper boundaries

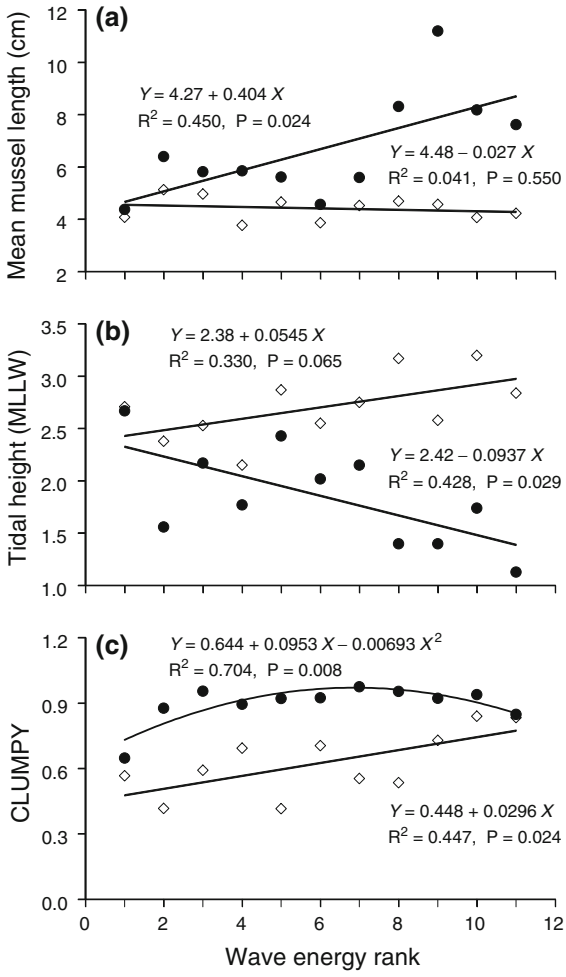

Fig. 9 **a**, **b**, **c** Regression analyses for field mosaics from the among-sites sampling scale. *Dots* = lower boundary estimates, *diamonds* = upper boundary estimates. **a** mean state (cm); **b** boundary height (meters above MLLW); **c** CLUMPY

were low, but increased with wave energy, approaching the high values of the corresponding lower boundaries (Fig. 9c).

Discussion

Size-dependent neighborhood processes and landscape patterns of boundary intensity

Without the neighborhood processes, one would expect to observe landscape patterns of boundary intensity commensurate with the spatial clines in the vital rates: gradual environmental gradients should produce diffuse boundaries; steep gradients should produce relatively intense boundaries (discussion in Turner 1989). This was evident in the within-site model without neighborhood processes (Fig. 5): Upper and lower boundaries show the same positive relationship between boundary intensity and wave energy (Fig. 5c). The trend arises because peak recruitment occurs at mid-shore levels of the most wave-exposed extremity, and consequently, vertical clines in recruitment become progressively steeper with increasing wave energy. The vertical clines were measured as the per cent change in recruitment within a frame from the proximal side (set in $\geq$90% cover) to the distal side (set in $\leq$10% cover). The clines ranged among frames of the upper boundary from 21% to 97% over the span from lowest to highest wave energies. Similarly, the clines in recruitment ranges among frames of the lower boundary from 47 to 97%. Regressions of CLUMPY on the per cent change are significant for both boundaries (upper boundary $F = 6.270$, df $= 1$, $P = 0.023$, multiple R squared $= 0.270$; lower boundary $F = 26.450$, df $= 1$, $P = 0.000$, multiple R squared $= 0.610$). The vertical clines of the other vital rates (predation, growth, and background mortality) do not vary over the wave energy gradient.

Adding facilitating neighborhood processes increases boundary intensities over the horizontal gradient of wave energy. For the within-site model without neighborhood processes, both boundaries ranged in intensity from approximately 0.0 to 0.3 (Fig. 4c), corresponding to random and near random dispersion of occupied cells. Including neighborhood processes in the within-site model boosted CLUMPY from approximately 0.2 to 0.7 for the upper boundary over the wave gradient, and 0.1 to 0.9 for the lower boundary, the latter value approaching the theoretical maximum of a perfectly aggregated distribution. Similar ranges occurred in the among-site version (Fig. 7c).

The real trends in boundary intensity captured in the mosaics were roughly similar to those of the corresponding models (Fig. 8c for within-site trends, Fig. 9c for among-site trends). Both boundaries showed some degree of aggregation, but lower boundaries were markedly more intense than upper boundaries, reaching values near the theoretical maximum. This outcome is consistent with the proposition that shore level differences in the crucial

ecological rates generated neighborhood effects that differed in intensity and mechanism.

One might ask whether abrupt lower boundaries could arise directly from sea star foraging patterns without recourse to neighborhood processes. Sea stars move up-shore with the flood tide to encounter prey (Robles et al. 1995). From the perspective of optimum foraging theory, it seems reasonable that once they encounter prey, all in the immediate vicinity should be removed, rather than rejected in favor of prey higher on the shore with the additional costs of travel. One might image, therefore, that an advancing front of sea stars alone is responsible for abrupt lower boundaries, which often occur as a change in cover from bare rock to 100% mussels over a distance less than the diameter of an average sized sea star.

Our studies do not support this explanation. Maintained by equilibrium processes (Robles et al. 2009), the lower boundary remains stationary throughout the sea stars' active season and from year to year (Paine 1974; Robles et al. 1995). However, its composition shows changes in response to experimental manipulations that are consistent with the argument for neighborhood effects. The lower margins of mussel beds usually consist of a layer of large mussels, which is resistant to predation, and from the surface of which smaller, vulnerable mussels have been browsed away, leaving other small mussels secreted underneath. Such sea star browse zones may be observed in the lower portion of mussel beds throughout the Pacific Northwest, but their width and conspicuousness vary with several factors, including apparent inter-annual and seasonal variation in mussel recruitment. Experimental removal of sea stars allows masses of new recruits to grow on top of the large mussels, and this cover of small mussels also extends down-shore to the rock surface below the original level of the lower boundary, but in comparatively diffuse array. As these mature, a diffuse boundary forms below the original. Once sea star removals are halted, small mussels unprotected by the cover of larger mussels are again browsed away restoring an abrupt boundary of large mussels (Fong and Robles, unpublished data).

Thus, energy/time considerations surely do underpin the mechanisms maintaining the lower boundary, but these relationships do not play out in so simple a way as a sharp front of extirpation, but rather through spatial dynamics that include the neighborhood processes.

Although diffuse relative to the lower boundaries, the upper boundaries in both the complete models and the mosaics are markedly more intense than the simulation without neighborhood processes. As with lower boundaries, neighborhood effects appear to have elevated boundary intensity, but to a lesser degree. Above the shore levels of the upper boundary, high temperature and desiccation are thought to be lethal for all sizes/ages, but within the boundary itself these stresses are believed to kill only solitary juveniles, while the moist microclimate around established mussels provides protection to newly settled juveniles (Connell 1972; Bertness and Leonard 1997; Harley and Helmuth 2003; Harley 2007).

These neighborhood processes were approximated by the model parameters. At high shore levels of the simulated landscapes, predation was minimal relative to background mortality, which included physical stress. The neighborhood weighting for recruitment rates was computed for juveniles 1 mm long, the equivalent of some weeks past settlement. The weak positive effect on recruitment of a neighborhood of small mussels mimics the protection afforded by the moist "footprint" of established mussels, but does not distinguish it from elevated settlement on or near the small adults. Available field data do not allow us to estimate the relative contributions to the neighborhood process of these two mechanisms.

A related consideration is the possible effects on recruitment of the patchwork covers of algae and other sedentary invertebrates that are evident in most of the mosaics of the upper boundaries. One would expect this cover to retain moisture and facilitate early survival of solitary mussels, promoting diffuse mussel covers without aggregation. Thus, community interactions that were not part of model assumptions may have contributed to the relatively low values of CLUMPY for upper boundaries in both the within- and among-site mosaics. We note, however, that some of the mosaics had little cover of the other species yet showed fragmented mussel boundaries relative to the corresponding length of lower boundary below. The low values of CLUMPY in these cases arose from fragmented irregular aggregations, i.e. clumps of multiple mussels, rather than many solitary mussels or small groups. Such a pattern is consistent with low settlement rates combined with

neighborhood effects on mortality from physical stress (see the next section for further discussion of the mechanism of upper boundaries).

Wilson and Agnew 1992 and Bruno et al. 2003 describe numerous possible cases of facilitating neighborhood effects in terrestrial plant, marine benthic, and tidal marsh communities. Many of these species (1) show recruitment and growth responses controlled by environmental factors and (2) are subjected to size-dependant interactions. Therefore, the hypothesis that facilitating neighborhood effects based on size-dependent interactions generate pronounced landscape patterns of boundary intensity seems broadly applicable.

Discrepancies between simulated and observed trends

The parameterization of the model is highly simplified for most processes, assuming linear relationships when the available data indicate only a direction of change, rather than a functional form. Thus, the models do not completely describe the complex dynamics of boundary formation, and the resulting discrepancies between simulated and real trends point the direction of further studies.

For example, in both models and mosaics CLUMPY values rise along the length of a given boundary from low to high wave energy (Figs. 3a,c, 6a,c, 8a,c, 9a,c). In the models these trends result from the steepness of the recruitment clines, as described above, and from the weighting of the neighborhood effect by the sum of the sizes of the surrounding mussels. Consequently, boundary intensities in the models are very sensitive to the increasing growth rates along the horizontal axis. Mean state and CLUMPY are strongly correlated for both models (Pearson $r = 0.87$, $P = 0.001$ and $r = 0.77$, $P = 0.009$, for upper and lower boundaries respectively in the within-site version; Pearson $r = 0.81$, $P = 0.000$ and $r = 0.77$, $P = 0.010$, for upper and lower boundaries in the among sites version). Thus, in the complex spatial process of the simulations spatially varying growth rates leverage the degree of neighborhood effect along a given boundary.

The trends in the mosaics did not, however, show a similar coupling of mean mussel size and boundary intensity. This is especially true of the upper boundaries. Over the gradient of increasing wave energy, neither within-sites or among sites mosaics showed a change in the stunted size of mussels over the wave energy gradient (Figs. 8a and 9a). However, intensities increased 0.3 units of CLUMPY for both (Figs. 8c and 9c). The independence of mean size and CLUMPY along upper boundaries suggests other factors influence the alongshore trend in intensity. Given the preceding discussion of the interspecific facilitation of recruitment, as well as the analysis of the model without neighborhood effects, a reasonable starting point for further study would be a field survey from sheltered to wave exposed locations looking for (1) a decrease in associated species (2) an increase in the vertical clines of recruitment, or (3) an increase in the severity of physical stress as boundaries rise.

Along the lower boundaries of both mosaic sampling scales, mean size and intensity increased with wave energy (Figs. 8c and 9c). However, mean size and intensity are significantly correlated only for the lower boundary of the with-in site mosaic (Pearson $r = 0.67$, $P = 0.048$); the correlation for the among-sites sample is weak ($r = 0.33$, $P = 0.325$). The apparent insensitivity of intensity to size in the among-sites sample may be merely a result of the small sample size, but other explanations are plausible. All but the lowest wave energy site had mean sizes >5 cm, at which mussels have attained a measure of resistance to predators. Further increases in size may impart little more positive effect in the neighborhood process.

A different aspect of the simplified neighborhood parameterization may explain another discrepancy between simulated and observed trends, as well as the apparent insensitivity of boundary intensity. The model assumes mussel beds occur as a single layer. In reality, mussel beds are several layers thick, except near the upper boundary, where the cover thins to a monolayer. The assumption of a monolayer causes the simulated high cover areas to appear porous (Figs. 2, 4, 6) as stochastic predation and other sources of morality empty cells. In real mussel beds, the loss of mussels from superficial layers of the bed does not clear the rock surface, except near the upper boundary. Therefore, layering might sustain recruitment and high coverage further into the low wave energy potion of the horizontal gradient, raising boundary intensity. This appears to explain a discrepancy between the shapes of

simulated and real curves for CLUMPY: in the models, the rise in CLUMPY with wave energy is gradual and obviously curvilinear, whereas in the mosaics the points at minimum wave energy are low outliers to linear fits of CLUMPY (Figs. 8c, 9c). Such an effect would also obviate a linear increase in the strength of neighborhood processes with mussel size.

Coda

Classical studies of population limitation on rocky shores were concerned with identifying a key factor setting a given boundary. This aim required little more than confirmation of a major source of mortality operating at the level of the boundary. The recent advent of spatial models and their pairing with practical techniques of landscape ecology promises a sea change in the investigative process (Paine 2002; Fagan et al. 2003; Hinchley et al. 2007). The approach requires explicit statement of assumptions, which includes characterization of crucial ecological rates at several scales, but in return facilitates a detailed analysis of complex landscape patterns and their formative dynamics. It offers the conspicuous advantage of a wealth of predictions that in their specificity are vulnerable to contradiction. As a case in point, we note the CA model's prediction of an alongshore rise in intensity for both upper and lower boundaries and its confirmation in the field were unanticipated outcomes. In turn, discrepancies between shapes of predicted and observed intensity curves indicated certain limitations of model assumptions and suggested roles for mussel layering, steeping environmental gradients, or interspecfic facilitation, depending on the circumstance. By providing a structured confrontation of manifold concepts and experience, the model-mosaic dialog quickened our understanding of complex spatial processes.

Acknowledgments Drafts of the manuscript were improved by D. Jelinski, J. van de Koppel, W. Wilson, and an anonymous reviewer. D. Fuentes assembled the mosaics and assisted other aspects of spatial analysis. Field assistants included C. Carrion, D. Fuentes, A. Martinez, and N. Sarkisian. We appreciate the assistance of the staff of the Bamfield Marine Sciences Centre. This work was supported by National Science Foundation Grants #RUI0089842, #HRD9805529, and #EF0827595. The fieldwork complied with the laws of Canada.

References

Bell EC, Denny MW (1994) Quantifying "wave exposure": a simple device for recording maximum velocity and results of its use in several field studies. J Exp Mar Biol Ecol 181:9–29

Bertness MD, Grosholtz E (1985) Population dynamics of the ribbed mussel, *Geukensia demissa*: the costs and benefits of an aggregated distribution. Oecologia 67:192–204

Bertness MD, Leonard GH (1997) The role of positive interactions in communities: lessons from intertidal habitats. Ecology 7:1976–1989

Blakeway DR, Robles CD, Fuentes DA, Qiu H-L (2004) Spatially extensive high resolution images of rocky shore communities. In: Seurant L, Strutton P (eds) Handbook of scaling methods in aquatic ecology: measurement, analysis, simulation. CRC Press, New York, pp 109–124

Bruno JF, Stachowicz JJ, Bertness MD (2003) Inclusion of facilitation into ecological theory. Trends Ecol Evol 18:119–125

Connell JH (1972) Community interactions on marine rocky intertidal shores. Annu Rev Ecol Syst 3:169–192

Dehnel PA (1956) Growth rates in latitudinally separated populations of *Mytilus californianus*. Biol Bull 110:43–53

Donalson DD, Desharnais RA, Robles CD, Nisbet RM (2004) Chapter 27: spatial dynamics of a benthic community. In: Seuront LaPGS (ed) Handbook of scaling methods in aquatic ecology: measurement, analysis, simulation. CRC Press, Boca Raton, pp 429–444

Fagan WF, Fortin MJ, Soykan C (2003) Integrating edge detection and dynamic modeling in quantitative analyses of ecological boundaries. Bioscience 53:730–738

Gordon AD (1999) Classification, 2nd edn. Chapman and Hall/CRC, Boca Raton

Gosz J (1993) Ecotone hierarchies. Ecol Appl 3:369–376

Guichard F, Halpin PM, Allison GW, Lubchenco J, Menge BA (2003) Mussel disturbance dynamics: signatures of oceanic forcing from local interactions. Am Nat 161:889–904

Harley CDG (2007) Zonation. In: Denny M, Gaines SD (eds) Encyclopedia of tidepools and rocky shores. University of California Press, Berkeley, pp 647–653

Harley CDG, Helmuth BST (2003) Local- and regional-scale effects of wave exposure, thermal stress, and absolute versus effective shore level on patterns of intertidal zonation. Limnol Oceanogr 48:1498–1508

Hinchley E, Nicholson M, Zajac R, Irlandi E (2007) Preface: marine and coastal applications in landscape ecology. Landscape Ecol doi:10.1007/s10980-007-9141-3

Kopp JC (1979) Growth and the intertidal gradient in the sea mussel *Mytilus californianus* Conrad, 1837. Veliger 22:51–56

Legendre P, Fortin MJ (1989) Spatial pattern and ecological analysis. Vegetatio 80:107–138

McGarigal K, Cushaman SA, Neel MC, Ene E (2002) FRAGSTATS: spatial pattern analysis program for categorical maps. Computer software produced by the authors at the University of Massachusetts, Amerherst, Massachusetts, USA. Available at www.umass.edu/landeco/research/fragstats/fragstats.html

Neel MC, McGarigal K, Cushaman SA (2004) Behavior of class-level landscape metrics across gradients of class aggregation and area. Landscape Ecol 19:435–455

Nielson KJ, Franz DR (1995) The influence of adult conspecifics and shore level on recruitment of the ribbed mussel *Geukensia demissa* (Dillwyn). J Exp Mar Biol Ecol 188:89–98

O'Neill R, Johnson A, King A (1989) A hierarchical framework for the analysis of scale. Landscape Ecol 3:193–205

Paine RT (1974) Intertidal community structure: experimental studies on the relationship between a dominant competitor and its principal predator. Oecologia 15:93–120

Paine RT (2002) Advances in ecological understanding: by Kuhnian revolution or conceptual evolution? Ecology 83:1553–1559

Risser PG (1995) The status of the science examining ecotones. Bioscience 45:318–325

Robles CD, Desharnais RA (2002) History and current development of a paradigm of predation in rocky intertidal communities. Ecology 83:1521–1537

Robles C, Sweetnam DA, Dittman D (1989) Diel variation in intertidal foraging of *Cancer productus* L. in British Columbia. J Nat His 23:1041–1049

Robles C, Sherwood-Stephens R, Alvarado M (1995) Responses of a key intertidal predator to varying recruitment of its prey. Ecology 76:565–579

Robles CD, Desharnais RA, Garza C, Donahue MJ, Martinez CA (2009) Complex equilibria in the maintenance of boundaries: experiments with mussel beds. Ecology 90:985–995

Strayer DL, Power ME, Fagan WF, Pickett STA, Belnap J (2003) A classification of ecological boundaries. Bioscience 53:723–729

Turner G (1989) Landscape ecology: the effect of pattern on process. Annu Rev Ecol Syst 20:171–197

van de Koppel J, Rietkerk M, Dankers N, Herman P (2005) Scale-dependent feedback and regular spatial patterns in young mussel beds. Am Nat 165:E66–E77

Vandermeer J, Yodis P (1999) Basin boundary collision as a model of discontinuous change in ecosystems. Ecology 80:1817–1827

Wilson JB, Agnew ADQ (1992) Postive feedback switches in plant communities. Adv Ecol Res 23:263–336

Wilson WG, Nisbet RM (1997) Cooperation and competition along smooth environmental gradients. Ecology 78:2004–2017

Wilson WG, Nisbet RM, Ross AH, Robles CD, Desharnais RA (1996) Abrupt population changes along smooth environmental gradients. Bull Math Biol 58:907–922